ISSN 1674-1056
http://cpb.iphy.ac.cn
http://iopscience.iop.org/cpb
中国物理 B
Chinese Physics
中国物理
Chinese Physics B

Compact wide stopband superconducting bandpass filter using modified spiral resonators with interdigital structure

Di Wu(吴荻), Bin Wei(魏斌), Bo Li(李博), Xubo Guo(郭旭波), Xinxiang Lu(卢新祥), Bisong Cao(曹必松)
Citation: Chin. Phys. B . 2018, 27(6): 068502. **doi:** 10.1088/1674-1056/27/6/068502

Journal homepage: http://cpb.iphy.ac.cn; http://iopscience.iop.org/cpb

What follows is a list of articles you may be interested in

Compact high-order quint-band superconducting band-pass filter

Di Wu(吴荻), Bin Wei(魏斌), Xi-Long Lu(陆喜龙), Xin-Xiang Lu(卢新祥), Xu-Bo Guo(郭旭波), Bi-Song Cao(曹必松)
Chin. Phys. B . 2018, 27(6): 068503. **doi:** 10.1088/1674-1056/27/6/068503

Compact superconducting single-and dual-band filter design using multimode stepped-impedance resonator

Xiang Wang(王翔), Bin Wei(魏斌), Xi-Long Lu(陆喜龙), Xu-Bo Guo(郭旭波), Bi-Song Cao(曹必松)
Chin. Phys. B . 2017, 26(12): 128501. **doi:** 10.1088/1674-1056/26/12/128501

High-temperature superconducting filter using self-embedding asymmetric stepped impedance resonator with wide stopband performance and miniaturized size

Dan Wang(王丹), Bin Wei(魏斌), Yong Heng(衡勇), Bi-Song Cao(曹必松)
Chin. Phys. B . 2017, 26(10): 108502. **doi:** 10.1088/1674-1056/26/10/108502

Superconducting tunable filter with constant bandwidth using coplanar waveguide resonators

Ying Jiang(蒋莹), Bo Li(李博), Bin Wei(魏斌), Xu-Bo Guo(郭旭波), Bi-Song Cao(曹必松), Li-Nan Jiang(姜立楠)
Chin. Phys. B . 2017, 26(10): 108501. **doi:** 10.1088/1674-1056/26/10/108501

A high-temperature superconducting filter withcontrollable transmission zero

Tianqi Gao(高天琪), Bin Wei(魏斌), Yong Heng(衡勇)
Chin. Phys. B . 2017, 26(5): 058503. **doi:** 10.1088/1674-1056/26/5/058503

Compact wide stopband superconducting bandpass filter using modified spiral resonators with interdigital structure*

Di Wu(吴荻)[1], Bin Wei(魏斌)[1,†], Bo Li(李博)[1], Xu-Bo Guo(郭旭波)[1], Xin-Xiang Lu(卢新祥)[2], and Bi-Song Cao(曹必松)[1]

[1] *State Key Laboratory of Low-Dimensional Quantum Physics, Department of Physics, Tsinghua University, Beijing* 100084, *China*
[2] *Department of Physics and Electronic Engineering, Shaoxing University, Shaoxing* 312000, *China*

(Received 31 January 2018; revised manuscript received 26 March 2018; published online 10 May 2018)

In this study, we propose a novel resonator that is composed of a modified spiral with an embedded interdigital capacitor. A large ratio of the first spurious frequency to the fundamental resonant frequency is obtained, which is suitable for the design of filters with wide stopbands, and the circuit size is considerably reduced by embedding the interdigital structure in the spiral. For demonstration, a compact four-pole high temperature superconducting (HTS) filter with a center frequency of 568 MHz is designed and fabricated on double-sided YBCO film with a size of 11.4 mm×8.0 mm. The filter measurement shows excellent performance with an out-of-band rejection level better than 60.9 dB up to 3863 MHz.

Keywords: high-temperature superconducting, bandpass filter, microstrip filter, wide stopband

PACS: 85.25.–j **DOI:** 10.1088/1674-1056/27/6/068502

1. Introduction

Bandpass filters (BPFs)[1–3] with compact size and high selectivity play an important role in wireless communication systems. Microstrip BPFs have attracted a great deal of attention from researchers, due to their planar structure and easy design procedures. However, undesired spurious bands and harmonics are unavoidable for frequency responses of BPFs. Wide stopband BPF should be developed to improve the signal quality through suppressing the interference from other wireless systems.

Several methods have been developed to improve the stopband performances of microstrip bandpass filters, and can be classified as two categories in general. The first category is to suppress unwanted harmonics. In Ref. [4], three ring resonators were used to generate the band-stop effect to suppress spurious responses. Defected ground structures[5] and a modified coplanar waveguide structure[6] were also adopted in the filter designs to provide transmission zeros in spurious frequencies. However, extra structures may aggravate insertion loss and increase circuit size. The second category is to improve the spurious responses of the resonator. Many resonators, such as quarter-wavelength resonators,[7] quarter-wavelength stepped-impedance resonators (SIRs),[8] asymmetric resonators,[9] asymmetric SIRs,[10,11] and interdigital resonators,[12] have been reported in constructing wide stopband filters.

Since the radio-frequency surface resistance of the high temperature superconducting (HTS) thin film is much smaller than that of normal metal film, HTS filters have attractive characteristics of low insertion loss, high out-of-band rejection, and high selectivity. Several HTS filters have been developed for microwave devices. In Ref. [13], quasi-lumped element resonators, comprising double-spiral inductors and interdigital capacitors, were used to increase the lowest harmonic to approximately triple the center frequency. Modified resonators with interdigital fingers and vertical meander line[14] were proposed in designing a wide stopband HTS filter, which has a first spurious frequency that is 5.2 times the center frequency.

In this work, a novel resonator with an interdigital capacitor embedded in a modified rectangular spiral is proposed. The resonator has a compact size and a first spurious frequency higher than 6.96 times the fundamental frequency. A four-pole HTS filter centered at 568 MHz with a −1-dB bandwidth of 14.5 MHz is designed and fabricated using the proposed resonator. The measurements accord well with the simulations. The filter exhibits good spurious suppression performance in terms of wide stopband and high rejection level.

2. Resonator design

2.1. Topology and resonant properties of the resonator

For the case of a half-wavelength rectangular-spiral resonator with a space in the middle, the potential distributions and the current directions at the fundamental resonant frequency and the first spurious frequency are shown in Figs. 1(a) and 1(b), respectively. At the fundamental resonant frequency, positive charges are concentrated at one end of the resonator,

*Project supported by the National Key Scientific Instrument and Equipment Development Project, China (Grant No. 2014YQ030975) and the National Natural Science Foundation of China (Grant Nos. 61371009 and 61401282).

†Corresponding author. E-mail: weibin@mail.tsinghua.edu.cn

© 2018 Chinese Physical Society and IOP Publishing Ltd

and negative charges are concentrated at the other end. The currents in spiral turns are in the same direction, and the space in the middle weakens the magnetic self-coupling field between the left and right turns significantly. Thus, the self-inductance of the resonator is increased, and the fundamental frequency is reduced. At the first spurious frequency, two ends of the resonator have the like charges, and the opposite charges are concentrated at the middle line of the resonator. Currents flow in different directions in the inner and outer turns of the spiral, so the inductance is reduced, and the first spurious frequency can be increased.

The charge distributions for an interdigital structure located at the end of a resonator are shown in Figs. 1(c) and 1(d). At the fundamental resonant frequency, the adjacent interdigital fingers concentrated with different charges enhance the self-capacitance. While at the first spurious frequency, the adjacent fingers concentrated with the like charges diminish the self-capacitance. Thus, the fundamental frequency is reduced, and the first spurious frequency is increased.

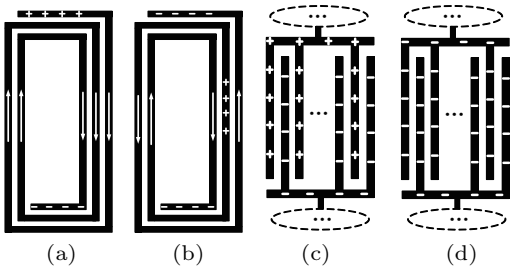


Fig. 1. Potentials (+ and −) and current directions (arrowed) of a rectangular-spiral resonator at (a) fundamental resonant frequency and (b) the first spurious frequency. Potential distributions of an interdigital structure located at the end of a resonator at (c) fundamental resonant frequency and (d) the first spurious frequency. Dashed ellipses represent other parts of the microstrip line of the resonator, and other fingers of the interdigital structure are represented by the ellipsis in the middle.

Figure 2 illustrates the proposed resonator, which is implemented by a modified spiral loaded with an interdigital capacitor. The resonator is based on three microstrip elements: an inductive spiral, capacitive pads grounding the resonator at two ends, and an interdigital capacitor. The outer end of the spiral is connected with the interdigital capacitor through air bridges as shown by grey curves in Fig. 2. In this work we utilize the apparently unused space in the center of the spiral, which exists in the original resonator structure. Compared with the traditional resonators that combine inductive and capacitive elements in parallel, the interdigital capacitor is embedded in the spiral through air bridges. Thus, the compactness of the resonator is enhanced.

The potential distributions and current directions in the fundamental and first spurious modes of the resonator are analyzed and shown in Figs. 2(a) and 2(b), respectively. At the fundamental resonant frequency f_0, the inductance of the spiral part and the capacitance of the interdigital part are both increased. This condition reduces frequency f_0. At the first spurious frequency, the inductance of the spiral part and the capacitance of the interdigital part are both diminished. Thus, the first spurious frequency f_s is increased, which leads to a large ratio f_s/f_0 and indicates that the proposed resonator is suitable for the design of wide-stopband filters. The currents mainly flow in the middle of the spiral lines and are small near the ends. Thus, the losses introduced by the air bridges are minimized.[15]

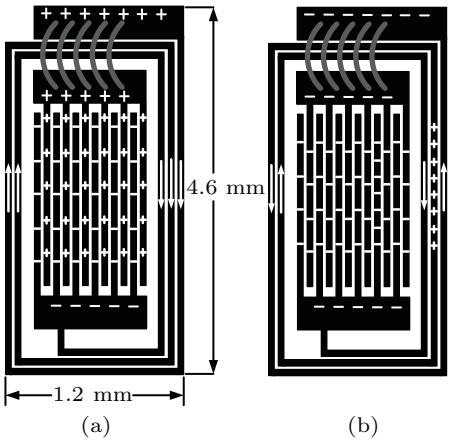


Fig. 2. Sketch of the proposed resonator (not to scale) with potentials (+ and −) and current directions (arrowed) at (a) fundamental resonant frequency f and (b) first spurious frequency f_s.

2.2. Parameters of the resonator

The line widths of the spiral and the interdigital fingers are all 0.04 mm, and the line spacing is 0.02 mm. Other parameters of the resonator are marked in Fig. 3(a). A full-wave electromagnetic (EM) simulation software Sonnet is used in this work. In the simulation, the substrate is set to be MgO with a thickness of 0.500 mm and a relative dielectric constant of 9.675. The entire resonator with a center frequency of 567.5 MHz is 4.6 mm×1.2 mm in size, and is compared by a double spiral-in-spiral-out (SISO) resonator and a meander-line resonator, which are loaded with the same interdigital

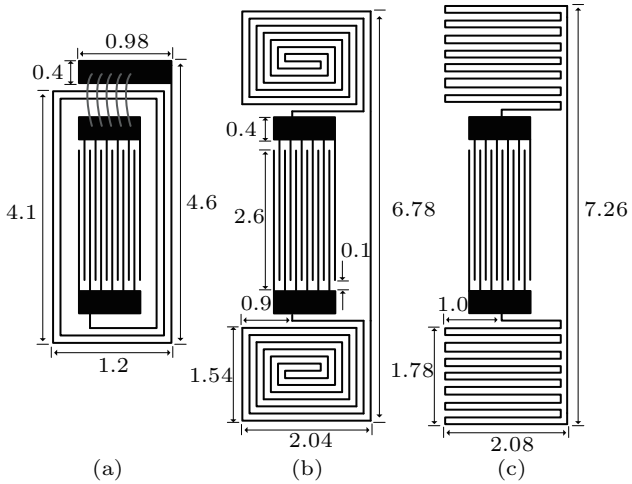


Fig. 3. Three different resonator structures (not to scale): (a) proposed spiral resonator, (b) double spiral-in-spiral-out (SISO) resonator, and (c) meander-line resonator loaded with the same interdigital capacitor. All dimensions are in unit mm.

capacitor as shown in Figs. 3(b) and 3(c). All three resonators are set to have the same fundamental frequency, line width, and line spacing. The comparison is shown in Table 1, in which we can see that the proposed resonator has the largest f_s/f_0 ratio of 6.96 and the most compact size.

Table 1. Comparisons of f_s/f_0 ratio and size among three resonator structures.

Resonator structure	f_0/MHz	f_s/f_0	Size/mm
(a)	567.5	6.96	1.20×4.60
(b)	567.5	2.08	2.04×6.78
(c)	567.5	3.91	2.08×7.26

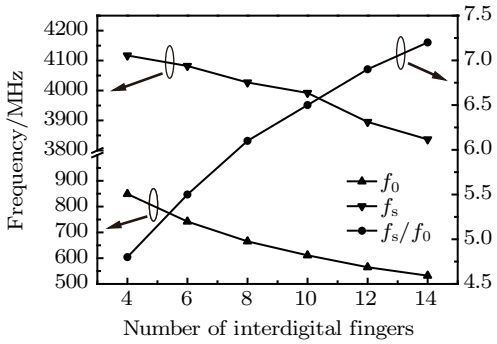


Fig. 4. Simulated resonant frequencies f, f_s, and f_s/f_0 ratio of the proposed resonator with different numbers of interdigital fingers.

The number of interdigital fingers plays an important role in achieving a high first spurious frequency. More fingers indicate a stronger capacitive effect of the interdigital structure. Figure 4 shows that the ratio of f_s/f_0 can be pushed up to 7 or more by increasing the number of interdigital fingers, while the spiral outside remains unchanged. However, many fingers require large spaces, which will increase the entire size of the resonator. Twelve interdigital fingers are used in this work with consideration of performance and overall size.

2.3. Coupling properties of the resonator

The coupling properties of the proposed resonators are simulated and analyzed. The electric fields are mostly concentrated between the interdigital fingers, which are surrounded by spiral lines. Very little electric field can leak into the space and this leads to a very weak electric coupling between resonators. By contrast, most of the magnetic energy is contained

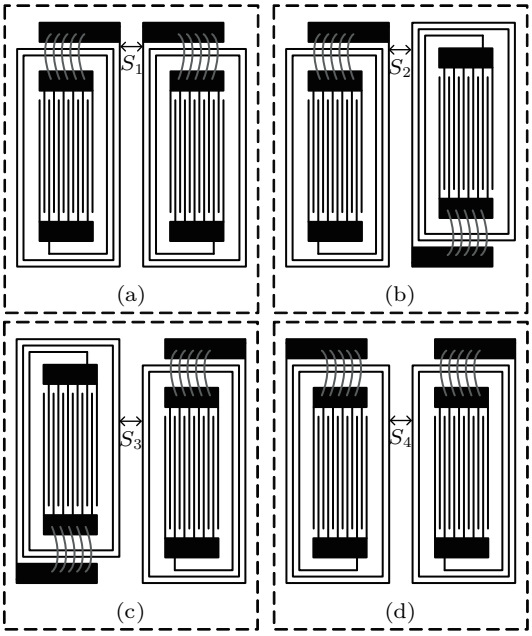


Fig. 5. Four types of coupling structures of the proposed resonators with different relative orientations.

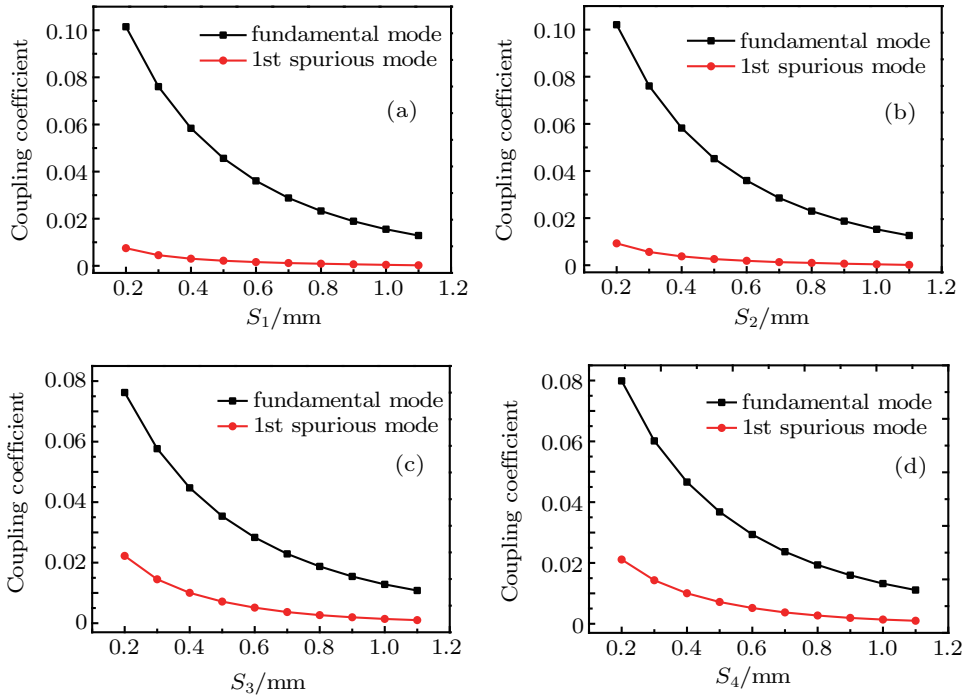


Fig. 6. (color online) Simulated coupling coefficients for four types of coupling patterns sketched in Fig. 5.

in the spiral lines. At the first spurious mode, the currents flow in opposite directions in the inner and outer turns of the spiral, resulting in a counteraction of magnetic fields in the space. Thus, the magnetic coupling between the resonators at the first spurious mode is weaker than that at the fundamental mode.

EM simulations are used to obtain the coupling coefficients. The simulated coupling coefficients as a function of distance between coupled resonators in patterns of Figs. 5(a) and 5(b), which are shown in Figs. 6 (a) and 6(b) respectively, are similar. The coupled structures shown in Figs. 5(c) and 5(d) also have approximate coupling function, as shown in Figs. 6(c) and 6(d), respectively. The coupling coefficients between the resonators in four patterns at the first spurious mode are all weaker than those at the fundamental mode. This feature is valuable for suppressing the spurious responses of BPF consisting of the proposed resonators.

3. Filter design, fabrication, and experiment performance

A four-pole Chebyshev filter centered at 568 MHz with a −1-dB bandwidth of 14.5 MHz is designed using the proposed resonators. The coupling structures in Figs. 5(b) and 5(c) are selected in the filter design. The orientations of adjacent resonators are opposite to each other in order to accommodate the tuning screws as shown in Figs. 7 and 8. The first and last resonator are connected to the input and output, respectively, by a winded high impedance line that has the same line width of 0.04 mm as the spirals to ensure external quality factor Q_e. The simulated performance of the filter is shown in Fig. 9 (dashed lines). The first spurious frequency is located at 3908 MHz, which is roughly 6.88 times the center frequency.

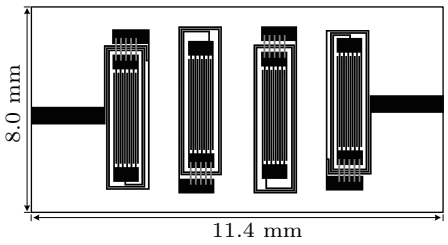


Fig. 7. Layout of the four-pole filter.

The four-pole HTS filter is fabricated on double-sided YBCO film deposited on a 0.5-mm-thick MgO substrate with a size of 11.4 mm×8.0 mm or $0.055\lambda_g \times 0.038\lambda_g$, where λ_g is the guide wavelength of the 50-Ω line on the substrate at the center frequency. The filter is patterned by standard photolithography and ion etching technology, and is packaged into a gold-plated shield box. Figure 8 shows the photograph of the fabricated filter with opened cover. To allow for further bonding, gold strips are left on the input/output feedlines and the pads at both sides of the air bridges. The AlSi bonding wires are used as air bridges to connect the outer end of the spiral with the interdigital capacitor.

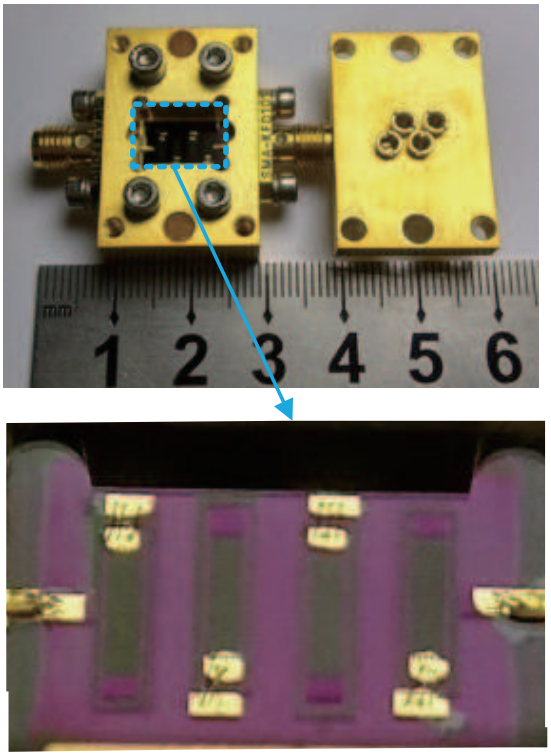


Fig. 8. (color online) Photograph of the fabricated HTS filter.

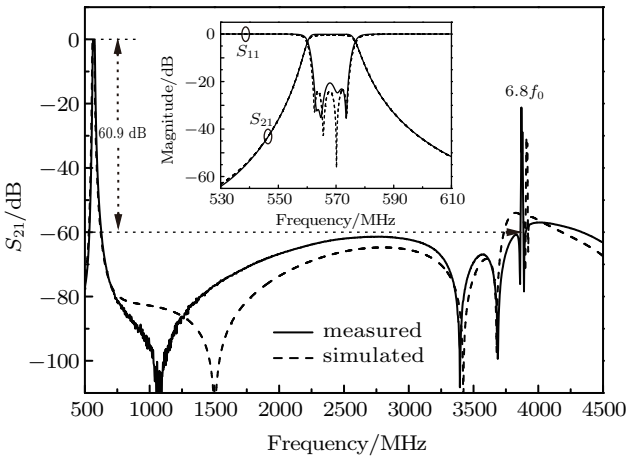


Fig. 9. Simulated and measured (after tuning) responses of the four-pole HTS filter.

The filter is cooled to 65 K through a Stirling cryocooler and measured by an Agilent E5072 A network analyzer with an input power of dBm. Four sapphire tuning rods are embedded in the cover of the shield box to optimize the passband response of the filter. The measured performances after tuning are shown in Fig. 9 (solid lines). The filter is centered at 568.3 MHz with a −1-dB bandwidth of 14.5 MHz. The measured in-band insertion loss including the bonding wires is less than 0.1 dB, and the measured return loss is greater than 20.5 dB. Figure 9 indicates that the upper stopband of the filter remains below 60.9 dB until 3863 MHz. Table 2 shows the comparison among HTS wide stopband filters, the filter proposed in this paper has a small size and exhibits good performance.

Table 2. Comparison among HTS wide stopband filters.

Ref.	Poles	f_0/MHz	Bandwidth/MHz	Rejection up to	Size (λ_g)
[10]	4	2400	247	4.4 f_0 (20 dB)	0.256×0.472
[11]	4	1112	10	3.7 f_0 (60 dB)	0.28×0.12
[14]	6	500	2	5.2 f_0 (75 dB)	0.17×0.05
This work	4	568	14.5	6.8 f_0 (60.9 dB)	0.055×0.038

4. Conclusions

A novel resonator composed of a modified spiral with an embedded interdigital capacitor has been proposed. A four-pole HTS filter centered at 568 MHz with a −1-dB bandwidth of 14.5 MHz is designed and fabricated using the proposed resonator. The filter has a compact size and a wide stopband. The measurements indicate that the upper stopband of the filter remains below 60.9 dB until 3863 MHz.

References

[1] Liu X Y, Zhu Lei and and Feng Y J 2016 *Chin. Phys. B* **25** 034101
[2] Zuo T, Zhao X J, Wang X K, Yue H W, Fang L and Yan S L 2009 *Acta Phys. Sin.* **58** 4194 (in Chinese)
[3] Cui B, Zhang X Q, Sun L, Bian Y B, Guo J, Wang J, Li C G, Li H, Zhang Q and He Y S 2010 *Chin. Sci. Bull.* **55** 1367
[4] Weng M H, Yang R Y, Hung C Y, Wu H W, Chen W N and Houng M P 2004 *Microw. Opt. Technol. Lett.* **43** 177
[5] Park J S, Yun J S and Ahn D 2002 *IEEE Trans. Microw. Theory Tech.* **50** 2037
[6] Lin L J, Ho M H and Xu W Q 2007 *Microw. Opt. Technol. Lett.* **49** 973
[7] Tang C, Lin X Q, Liu W M and Fan Y 2017 *IET Microw. Anten. Propag.* **11** 1379
[8] Kuo T N, Li W C, Wang C H and Chen C H 2008 *IEEE Microw. Wireless Compon. Lett.* **18** 389
[9] Tang C W and Hsu Y K 2008 *IEEE Microw. Wireless Compon. Lett.* **18** 91
[10] Liu H W, Ren B P, Li S, Guan X H, Wen P, Xiao X and Peng Y 2015 *IEEE Trans. Appl. Supercond.* **25** 1501606
[11] Wang D, Wei B, Heng Y and Cao B S 2017 *Chin. Phys. B* **26** 108502
[12] Tang C W and Liu W T 2008 *IEEE Microw. Wireless Compon. Lett.* **18** 767
[13] Zhou J F, Lancaster M J, Huang F, Roddis N and Glynn D 2005 *IEEE Trans. Appl. Supercond.* **15** 1004
[14] Wang J C, Wei, B, Cao B S, Zhang X P, Guo X B and Song X K 2013 *IEEE Trans. Appl. Supercond.* **23** 1502108
[15] Suo G N, Guo X B, Cao B S, Wei B, Zhang X P, Shang Z J and Zhang G Y 2014 *IEEE Trans. Appl. Supercond.* **24** 1501005